Utilization of FESS to Support an EV Smart Fast Charging Station Coupled to a Low-Inertia Grid: A South African Perspective

Willy S. Ngaha¹, Chandima Gomes¹, and David G. Dorrell^{2,1}

Abstract—Conventional internal combustion engine vehicles (ICEV) are among the main contributors to carbon emissions, which significantly damage the ozone layer. Although refueling such vehicles takes approximately one minute for 20 liters, enabling a travel range of about 100 km at a cost of roughly R400, the charging of electric vehicles (EVs) takes longer, which introduces new challenges. For the same travel distance, EVs typically require 40-60 minutes of charging at a cost of around R175 for a DC fast charging station (FCS). The rapid growth of electric vehicles (EVs) in South Africa is driving an urgent need for stable and energy-efficient charging infrastructures. This paper investigates the impact of flywheel energy storage systems (FESS) in developing smart EV fast-charging stations in a low-inertia grid. During peak demand periods, simultaneous charging of multiple EVs can result in low power density and sudden load disturbances. A hybrid energy system consisting of 10 MW grid supply, 1.25 MW from photovoltaic (PV) and wind energy conversion systems, and 15 FESS units rated at

100 kW each was modeled on Matlab /Simulink and validated on a Matlab m-file. To enhance stability, an asynchronous decentralized model predictive control (AD-MPC) approach was implemented to coordinate distributed energy storage during peak demand charging periods. Simulation on Matlab Simulink results demonstrated that the combined use of FESS and AD- MPC significantly reduced grid frequency deviation from 0.18

Hz (without FESS) to 0.06 Hz, while also decreasing charging time and improving power density. The findings confirm that FESS offers a high-power and fast response solution compared to conventional battery systems. The proposed framework provides a scalable pathway for low-carbon and resilient EV charging infrastructure, supporting South Africa's transition toward a sustainable energy future.

Index Terms—Flywheel Energy Storage System (FESS); Asynchronous Decentralized Model Predictive Control (AD-MPC); Electric Vehicle (EV) Fast Charging; Inverter-Based Resources (IBR); Frequency Stability; Power Density Enhancement; Smart Grid Integration; South African Energy Transition.

I. INTRODUCTION

The 21st century is characterized by ongoing challenge and transition between electric vehicles (EVs) and conventional internal combustion engine vehicles (ICEVs), driven by concerns over sustainability, energy efficiency, and environmental

¹School of Electrical and Information Engineering University of the Witwatersrand Johannesburg, South Africa

2492558@student.wits.ac.za; chandima.gomes@wits.ac.za; dgdorr@utu.fi

impact. The global transportation sector is undergoing a significant transformation with the rapid adoption of EVs. Compared to conventional ICEVs, EVs are widely regarded as a cost-effective and environmentally sustainable alternative, offering lower operating costs and reduced greenhouse gas emissions [1], [2]. South Africa, in particular, has begun to experience increased penetration of EVs in their grid and transportation systems, with government policies and private initiatives supporting the development of charging infrastructure [3], [4]. However, the expansion of EV adoption presents both opportunities and challenges for the stability of the national grid and traffic. Projections indicate that once EVs constitute around 65% of the vehicle fleet, significant stress will be placed on the power system if charging is not intelligently managed [5].

To address these challenges, advanced smart charging stations are required that can integrate inverter-based resources (IBRs) with energy storage technologies. IBRs integration provides an opportunity to supply cheaper, cleaner power, but intermittency and variability create uncertainties for grid stability [6]. In this context, flywheel energy storage systems (FESS) have emerged as an attractive solution due to their fast response times, high cycle life, and capability to handle short- duration power imbalances [7]. FESS can instantly absorb or release energy to stabilize the grid during sudden load fluctuations, such as peak EV charging demand [2], [5].

This paper proposes the development of a smart charging station model that incorporates both FESS and IBRs, as shown in Fig. 1, controlled by an AD-MPC. The FESS is designed to provide stabilization and frequency support to the EV-grid system during EV peak demand, while the IBRs ensure the operation of SCS at low cost. By combining these technologies, the proposed system aims to enhance the resilience of South Africa's EV charging infrastructure while maintaining affordability and sustainability for future large- scale EV adoption. The table presents a comparison of the different charging technologies and a Table I comparing the annual usage of EVs and ICEVs.

The remainder of this paper is structured as follows. Section

²Department of Mechanical and Material Engineering, University of Turku, Turku, Finland

TABLE I
COMPARISON OF ANNUAL USAGE BETWEEN EVS AND ICEVS

Vehicle Type	E (100 km)	E_{an}	Fuel Price	An Cost
EV (Public				
AC Charging)	16 kWh	2,400 kWh	R5.50/kWh	R13,200
EV (Public DC				
Fast Charging)	16 kWh	2,400 kWh	R9.00/kWh	R21,600
Petrol Car	7 L	1,050 L	R25.00/L	R26,250



Fig. 1. Image of hybrid smart EV fast charging stations

II provides a review of FESS with EV charging control methods. Section III presents the proposed AD-MPC strategy. Section IV describes mathematical modeling of the global grid system and the local FCS system. The case study is described in Section VI, the results are presented in Section VII, and the conclusion and recommendations for future directions are presented in Section VIII.

II. BRIEF LITERATURE REVIEW

A brief literature review was conducted to assess the current state of EV technology in South Africa and to identify the control methods currently being implemented in the charging infrastructure.

A. EV Companies Present in South Africa

These companies have manufacturing plants in SA, though many have not yet produced fully electric vehicles locally. Major automotive manufacturers operating in South Africa including BMW South Africa (BMWSA), Ford Motor Company of Southern Africa (FMCSA), Mercedes-Benz South Africa (MBSA), Volkswagen South Africa (VWSA), Nissan South Africa (NSA), Toyota South Africa Motors (TSAM), and Isuzu South Africa (ISA) have each introduced or announced their first EV models between 2013 and 2026 as shown in Table II-A, with production and market availability steadily accelerating, collectively, these initiatives are projected to contribute to a substantial increase in EV production and adoption in the country by 2030, with the passenger EV fleet expected to reach approximately 25,456 units, representing about 0.3 % of the total passenger vehicle in SA [8].

B. Review of EV Control Methods

According to [16], there is an increasing interest in researching and implementing FESSs in IBR situations. The study

TABLE II
PRINCIPAL EV MANUFACTURER AND THEIR LOCATION IN SOUTH AFRICA

Location in SA	Notes on EV / NEV involvement
Gauteng	BMW iX3, 2022
Gauteng	Ford Ranger PHEV
Eastern Cape	EQC 400 4MATIC, 2019
Eastern Cape	e-Golf pilot project. FEb. 2020
Gauteng	Nissan Leaf, 2013
KwaZulu-Natal	Toyota bZ4X, 2025
Eastern Cape	D-Max EV, 2026
	Gauteng Gauteng Eastern Cape Eastern Cape Gauteng KwaZulu-Natal

finds that FESSs have tremendous potential for improving grid stability. In [17], a droop-based control approach is used to coordinate an EV-FCS without using digital communication between the grid and FESS converters. The suggested method responds well to system-level inputs while remaining consistent with the EV battery's specified charging profiles. In [18], mixed integer linear programming (MILP) is utilized to study the economic efficiency of EV-FCS with increased battery-flywheel energy storage. The results show that the battery-flywheel enhanced FCSan can reach a net present value up to 12 % higher than that of system FCS without energy. In [19], a frequency regulation trial was conducted utilizing a hybrid energy storage system (HESS) consisting of a 1 MW flywheel and a 4 MW lithium battery.

The PSO algorithm was used to minimize wind-solar power fluctuation. HESS saves expenses by 45.1 % when compared to single-battery energy storage. This is one of the first initiatives in the world to apply the HESS model to an IBR, proving the viability of employing several storage technologies to smooth wind power variations. Recent innovations combine MPC and its derivatives, such as asynchronous decentralized MPC (AD-MPC), to boost the dynamic performance of WECS in hybrid renewable systems [20], [21]. When combined with FESS, these control techniques assist in reducing frequency deviations, increasing grid stability, and enabling high-power EV charging operations. Depending on the DC bus voltage variance and real-time grid demand at the charging station, the FESS can absorb (charge) or release (discharge) energy. Equation (1) provides the energy E_f of a FESS.

$$E_f = \frac{1}{2}J\omega_m^2 \tag{1}$$

where: ω_m represents the rotor speed driving the FESS, whereas J represents the machine's moment of inertia driving the flywheel. FESSs' major components include flywheel rotors, motor types, bearing support technologies, and power electronic converter technologies. In [22], FESSs are discussed in several contexts. The interest stems from an application involving a ride-connected electric vehicle charging station equipped with photovoltaic (PV) generators and an FESS EV. When the overall investment costs of two systems, the Bat-PVHS (battery and photovoltaic hybrid system) and the FL-PVHS (flywheel and photovoltaic hybrid system), are compared, the FL-PVHS has a somewhat lower total lifetime investment than the Bat-PVHS does.

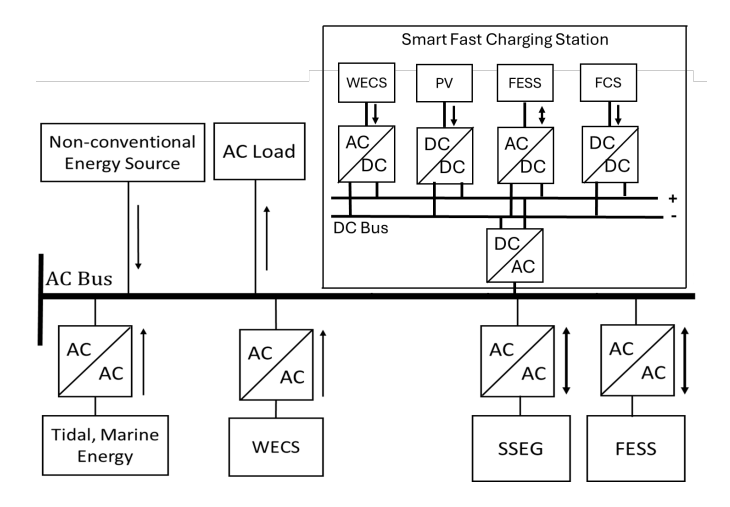


Fig. 2. Topology of the FESS, EV, and IBR coupled on the same DC bus

III. METHODOLOGY

It is reported in [23] that the increasing number of EVs in South Africa is estimated to exceed about 22,500 vehicles by 2030, which projects South Africa among the countries to cope with this technology. The intention is to develop a large-scale charging hub of approximately 35 fast chargers (FCS units) operating simultaneously, each rated at around 350 kW, and typically charge EVs for 20–40 minutes per session. The instantaneous power demand resulting can easily reach 12.5 MW, leading to rapid load fluctuations and stressing both the grid and the IBR on-site. To achieve this, it is necessary to predict the demand capacity of EV, which determines the choice of MPC. This MPC was used in [24] to control FESS for charge/discharge control. However, it does not explicitly combine EV charging and FESS in the same scenario.

The FCS control units (EV chargers, PV, WECS, and FESS subsystems) can update their decisions at different times or rates without global synchronization. This is particularly relevant in real charging environments, where communication delays can occur. This describes the asynchronous nature of the problem. Each local controller optimizes its charging or power exchange profile considering the station's power balance and renewable energy availability. Furthermore, the distributed framework ensures global coordination through limited information exchange, which describes the decentralized nature of the problem.

To effectively manage this complex, large-scale, and dynamic system, shown in Fig. 2, the local control of FCS is independent of the global control of the system. An asynchronous distributed model predictive control (AD-MPC) strategy is adopted. Unlike conventional centralized MPC, which requires global state information and synchronized communication, AD-MPC enables local controllers (e.g., each charger or energy storage unit) to operate semi-independently while exchanging limited information with their neighbors or a coordinator. This structure offers several key advantages for smart charging stations:

IV. MATHEMATICAL MODELING AND CONTROL FRAMEWORK

The swing equation (2) is the fundamental dynamic equation that describes how the rotor angle (frequency) of a synchronous machine responds to grid power imbalances.

$$\begin{cases} J.\frac{d\omega_m}{dt} + B.\omega_m = T_e - T_L \\ T_e = \phi_s.i_{abc} \\ \frac{d\delta}{dt} = \omega_i - \omega_j \end{cases}$$
 (2)

where: J,B,ω_m and T_L are the moment of inertia, the magnetic friction, the rotor speed, and the load torque, respectively. On this assumption, the measured voltage at the PCC can be regarded as the same as the voltage reference, that is $V_{pcc}=V_{ref}$, and $\theta_{pcc}=\theta_{ref}$. The linearized (Small-Signal) form of the (2) used in MATLAB/Simulink, for small-signal stability studies and control design, is given in (3).

$$\Delta \dot{\omega} = \frac{\omega_s}{2H} (\Delta P_m - \Delta P_e - D\Delta \omega) \tag{3}$$

A. Power Balance in the Smart Charging Station

At every time step t, the station must satisfy the power balance (4).

$$P_{PV}(t) + P_W(t) + P_{fl}(t) + P_g(t) = P_{EV}(t) + P_l(t)$$
 (4)

where $P_{PV}(t)$ and $P_W(t)$ represent IBR power inputs, $P_{fl}(t)$ is the power exchanged by the flywheel, and $P_g(t)$ is the grid import or export power. $P_{EV}(t)$ denotes the instantaneous EV charging load, and $P_l(t)$ includes converter and transmission losses. During charging or discharging, the FESS can act as both a power charging ($P_{fl} < 0$) or a power source discharging ($P_{fl} > 0$).

B. Conventional Synchronous Generator / Single Area LFC (basic blocks)

Let us consider the nonlinear swing equation, which mathematically represents the grid as shown in the (2), to define the classic swing equation used in LFC as shown in (5). Convert to power form (per-unit) using $(M=\frac{2H}{\omega_s})$ (or use (M) inertia constant in pu·s).

$$M\Delta\dot{\omega}(t) = \Delta P_m(t) - \Delta P_e(t) - D\Delta\omega(t) \tag{5}$$

considering the governor and the turbine as shown in the (6)

$$\begin{cases} \tau_g \Delta \dot{P}_g + \Delta P_g = -\frac{1}{R} \Delta \omega + \Delta P_c \\ \tau_t \Delta \dot{P}_m + \Delta P_m = \Delta P_g \end{cases}$$
 (6)

where R is the speed drop, (τ_g, τ_t) is the time constants of the governor and the turbine, and (ΔP_c) is the setpoint power.

The change in the tie-line $\Delta P_{tie,12}$ (two-area) linearization for two areas, tie-line power deviation (linearized), is given by (7).

$$\Delta P_{tie,12} = T_{12} \left(\Delta \delta_1 - \Delta \delta_2 \right) \tag{7}$$

where: T_{12} , $\Delta\delta_1$, $\Delta\delta_2$ are respectively the tie-line coefficient, the change in rotor of machine 1, and machine 2. Since $\Delta\dot{\delta}_i=\Delta\omega_i$, the tie-line couples the swing equations of two areas. Let us determine the small signal state space of the system by considering the small signal of a single area.

$$x = \begin{bmatrix} \Delta \delta & \Delta \omega & \Delta P_g & \Delta P_m \end{bmatrix}^T \tag{8}$$

then

$$\begin{cases} \Delta \dot{\delta} &= \Delta \omega \\ M \Delta \dot{\omega} &= -K_s \Delta \delta - D \Delta \omega + \Delta P_m - \Delta P_e^{\text{dist}} \\ \tau_g \Delta \dot{P}_g &= -\Delta P_g - \frac{1}{R} \Delta \omega + \Delta P_c, \\ \tau_t \Delta \dot{P}_m &= -\Delta P_m + \Delta P_g, \end{cases}$$
(9)

C. Development of the Wind Energy Conversion System (WECS)

The output from the generator is conditioned using a back-to-back converter to allow variable-speed operation and implement maximum power point tracking (MPPT), which ensures optimal energy capture at different wind speeds [25]. In South Africa, the adoption of WECS is gaining momentum as part of the transition toward IBR generation, especially for smart charging station integration [26]. Therefore, it is important to integrate the WECS in this project. Let us use a rotor-coupled (DFIG / SG) WECS has mechanical inertia with nonlinear aerodynamic mechanical power as shown in (10).

$$P_{m,w} = \frac{1}{2}\rho A C_p(\lambda, \beta), V_w^3 \tag{10}$$

where V_w is the wind speed, A is the area, λ is the tip-speed ratio, and(β) is the pitch coefficient.

Linearizing $P_{m,w}$ about the operating point gives the small signal mechanical power change as shown in the (11), with $K_{w\omega}$, $Delta\omega_w$, and ΔV_w , these voltage and speed coefficients.

$$\Delta P_{m,w} \approx K_{wv}, \Delta V_w + K_{w\omega}, \Delta \omega_w + \dots \tag{11}$$

Assuming the WECS is grid-connected through a DFIG, it contributes inertia (M_w) and damping (D_w) to the aggregated system. The small-signal swing contribution used in the ADMPC is given in (12).

$$M_w \Delta \dot{\omega} = \Delta P_{m,w} - \Delta P_{e,w} - D_w \Delta \omega \tag{12}$$

Pitch control and torque control dynamics can be modeled as additional first-order dynamics (time constants $(\tau_{pitch}, \tau_{tc})$).

D. Development of Photovoltaic (PV) Plant with Full Converter

The Photovoltaic (PV) plant plays a pivotal role in modern IBRs systems, providing a clean and sustainable source of electricity, despite having no rotating mass, no physical inertia [21]. In South Africa, where solar irradiance levels are among the highest globally (averaging 2200 kWh/m² per year), PV systems are a cornerstone for achieving decarbonization and supporting the integration of EV smart charging stations [27]. The rise of distributed energy resources and the integration of PV systems using advanced control strategies such as AD-MPC have been extensively investigated. These approaches enhance the stability, power quality, and load-following capability of PV plants, especially when coupled with FESS for transient smoothing and peak-shaving applications in EV fast-charging networks [20], [21]. Key dynamic elements, Power available (nonlinear) on PV solar, are given by the (13).

$$P_{PV}(t) = \eta A I(t) f(T, ...) \approx P_{PV0} + \frac{\partial P_{PV}}{\partial I} \Delta I(t)$$
 (13)

where I(t) is irradiance. The disturbance due to sudden cloud inverter control (small-signal), assuming the PV inverter implements droop/virtual inertia as shown in the (14).

$$\tau_{inv}, \Delta \dot{P}_{pv} + \Delta P_{pv} = -K_{pv}^{droop}, \Delta \omega + \Delta P_{ref} + G_I(s)\Delta I$$
(14)

where $G_I(s)$ maps irradiance variation to output power (fast). Without frequency control, the photovoltaic system is a disturbance injection as shown in (15).

$$\Delta P_{pv}(s) = G_I(s)\Delta I(s) \tag{15}$$

PV solar with grid-forming mode, if the PV solar inverter runs as a grid-forming source with virtual inertia M_{pv} as shown in the (16)

$$M_{pv}\Delta\dot{\omega} = \Delta P_{pv,ctrl} - D_{pv}\Delta\omega \tag{16}$$

with control dynamics τ_{inv} on the power setpoint. Practically, many PV plants can provide fast active power support via curtail/over-dispatch or droop emulation with sub-second dynamics.

E. Development of Small-Signal Linearization FESS Dynamic Model

The FESS is modeled as a Permanent Magnet Synchronous Motor (PMSM) coupled to a flywheel with inertia through a grid-forming converter, as shown in (17).

$$\begin{cases} J\Delta\dot{\omega}_r = -\left(\frac{P_{f0}}{\omega_{r0}^2} + B_f\right)\Delta\omega_r - \frac{1}{\omega_{r0}}\Delta P_f + \Delta T_m \\ \tau_c\Delta\dot{P}_f = -\Delta P_f + K_c\Delta u_f \end{cases}$$
(17)

FESS energy dynamics: energy decreases when discharging, and increases otherwise. Sign convention: $(P_f>0)$ means discharge supplying the DC bus; adjust the sign if you prefer the opposite

$$\dot{E}_f = -P_f \tag{18}$$

F. Development of EV Charging

A common, tractable EV battery model suitable for systemlevel control is the first-order equivalent circuit as shown in the (19)

$$\begin{cases} V_{bat}(t) = V_{oc}(SoC(t)) - R_{bat}I_{bat}(t) \\ C_{eq}\frac{dV_{oc}}{dt} = -\frac{I_{bat}(t)}{Q_{cap}} \implies \dot{SoC}(t) = -\frac{I_{bat}(t)}{Q_{cap}} \\ P_{ev}(t) = V_{bat}(t)I_{bat}(t) \end{cases}$$
(19)

Where: SoC is the state of charge (0–1), Q_{cap} is battery capacity (Ah), R_{bat} is the internal resistance, I_{bat} is charging current (A), $(V_{oc}(\cdot))$ is an open-circuit voltage vs SoC (nonlinear).

The global system is not part of this study; the development of the state, the input, the disturbances, and the output equation is left to the reader. Let's develop the EV fast charging station control by the AD-MPC. The state equation of the system can now be obtained by considering all injections into the swing equation (5), (6), (12), (14) aggregate single-area LF model, including IBRs and FESS, to obtain (20), which is determined by a matrix in x

$$M_{tot}\Delta\dot{\omega} = \Delta P_m^{(\text{conv})} + \Delta P_W + \Delta P_{pv} + \Delta P_{fl} - \Delta P_e - D_{tot}\Delta\omega$$
(20)

where: $M_{tot} = M_{sg} + M_w^{(\text{if emulated})} + M_{pv}^{(\text{if emulated})}$ (aggregate inertias), (D_{tot}) sums damping/droop, (ΔP_{fl}) is the flywheel injection (FESS), typically modeled as first order include both disturbance terms (wind/irradiance) and controlled responses (droop/emulation).

$$x = \begin{bmatrix} \Delta \delta & \Delta \omega & \Delta P_{fess} & \Delta P_m & \Delta P_{pv} & \Delta P_{wec} \end{bmatrix}^T$$

$$\dot{x} = \begin{bmatrix} 0 & 1 & 0 & 0 & 0 & 0 \\ -\frac{K_s}{M_{tot}} & -\frac{D_{tot}}{M_{tot}} & \frac{1}{M_{tot}} & \frac{1}{M_{tot}} & \frac{1}{M_{tot}} & \frac{1}{M_{tot}} \\ 0 & 0 & -\frac{1}{\tau_f} & 0 & 0 & 0 \\ 0 & 0 & 0 & -\frac{1}{\tau_t} & 0 & 0 \\ 0 & 0 & 0 & 0 & -\frac{1}{\tau_{inv}} & 0 \\ 0 & 0 & 0 & 0 & 0 & -\frac{1}{\tau_{inv}} \end{bmatrix}$$

where inputs (u) include control commands to the turbine, FESS, PV/WECS setpoints; disturbances (w) include irradiance, EV charging, and wind speed deviations.

G. Mathematical Modeling of EV Fast Charging Station

Let represent the active set of chargers by $\mathcal{A}(t)$, the EV charging power is defined as $P_{EV}(t) = \sum_{i \in \mathcal{A}(t)} P_{ch,i}(t)$. The DC bus voltage V_{dc} dynamics shown in Fig. 2 is given by (21). The station level power balance (instantaneous) is given in (22).

$$\begin{cases}
C_{dc}\dot{V}_{dc}(t) = \frac{1}{V_{dc}(t)} \left(P_{g,dc} + P_{PV,dc} + P_{W,dc} + P_{fl,dc} - \sum_{i} P_{ch,i} - P_{l} \right) \\
- \sum_{i} P_{ch,i} - P_{l} \right)
\end{cases}$$
(21)

$$\begin{cases} P_g(t) + P_{PV}(t) + P_W(t) + P_{fl}(t) = \sum_{i=1}^{N_{ch}} P_{ch,i}(t) \\ + P_{aux}(t) + P_l(t) \end{cases}$$
(22)

AD-MPC design the prediction model uses linearized (A_d, B_d) . The terminal constraint/penalty enforces the minimum SoC objective. Robustness: tube-MPC or constraint tightening to handle asynchrony and IBRs uncertainty. This is the core equality the AD-MPC must satisfy or manage via controlled grid import $P_g(t)$, FESS dispatch (P_{fl}) , and charger setpoints $(P_{ch,i})$. The EV model is as follows.

- 1) State, Input, and Disturbance Vectors:
- States:

$$\begin{bmatrix} \Delta V_{dc} & \Delta P_f & \Delta E_f & \Delta P_{EV} \end{bmatrix}^T$$

• Inputs (control):

$$u = \begin{bmatrix} \Delta P_g & \Delta u_f & \Delta P_{EV}^{cmd} \end{bmatrix}^T$$

where Δu_f is the FESS power command and (ΔP_{EV}^{cmd}) is the aggregate charger power command from the station controller.

Disturbances:

$$w = \begin{bmatrix} \Delta P_{pv} & \Delta P_w & \Delta P_{loss} \end{bmatrix}^T$$

• Outputs:

$$y = \begin{bmatrix} \Delta V_{dc} & \Delta P_{EV} & \Delta f \end{bmatrix}^T$$
 (choose as needed).

Nonlinear (physical) equations base relations: DC bus energy/voltage dynamics is obtained by an approximate energy form. $V_{dc}(t) \approx V_{dc0}$ of (21), so factor $1/V_{dc0}$ is constant. Aggregate charger dynamics (power tracking) as shown in (23)

$$\tau_{ch}, \dot{P}_{EV} + P_{EV} = P_{EV}^{cmd} \tag{23}$$

Linearize around the equilibrium and write in compact form:

$$\dot{x} = Ax + Bu + Ew$$

With the chosen states, the matrices are:

$$A = \begin{bmatrix} -\frac{1}{C_{dc}V_{dc0}} \frac{\partial P_{loss}}{\partial V_{dc}} & \frac{1}{C_{dc}V_{dc0}} & 0 & -\frac{1}{C_{dc}V_{dc0}} \\ 0 & -\frac{1}{\tau_f} & 0 & 0 \\ 0 & -1 & 0 & 0 \\ 0 & 0 & 0 & -\frac{1}{\tau_{ch}} \end{bmatrix}$$

$$B = \begin{bmatrix} \frac{1}{C_{dc}V_{dc0}} & 0 & 0\\ 0 & \frac{K_f}{\tau_f} & 0\\ 0 & 0 & 0\\ 0 & 0 & \frac{1}{\tau_{ch}} \end{bmatrix}$$

$$E = \begin{bmatrix} \frac{1}{C_{dc}V_{dc0}} & \frac{1}{C_{dc}V_{dc0}} & -\frac{1}{C_{dc}V_{dc0}}\\ 0 & 0 & 0\\ 0 & 0 & 0 \end{bmatrix}$$

Outputs is
$$y=Cx$$
, with $y=[\Delta V_{dc},\ \Delta P_{EV}]^T$
$$C=\begin{bmatrix}1&0&0&0\\0&0&0&1\end{bmatrix}$$

V. ASYNCHRONOUS DECENTRALIZED MODEL PREDICTIVE CONTROL (AD-MPC)

The small signal of the local system is made of stack states $x = [\Delta SoC_i, \ \Delta V_{dc}, \ \Delta P_{fl}, \ \Delta \omega_g, \dots]$, linearize dynamics input u contains charger power commands and storage dispatch commands. This model can be used in discrete-time after sampling the MPC prediction model $x_{k+1} = Ax_k + Bu_k + Ew_k$. Each local agent (charger or storage) solves an objective function by minimizing J_i over horizon N_p as shown in (24), which is subject to the grid prediction model and constraints.

The AD-MPC optimizes each subsystem (PV, WECS, FESS, Grid) independently, ensuring coordination through iterative updates of the predicted states and charging buses, without requiring continuous communication. At each control interval k, each local controller i minimizes its own cost function.

$$\min_{P_{fl}(k), P_g(k)} J_i = \begin{cases} \sum_{i=k}^{k+N_p} w_1 (P_{EV}(i) - P_{sup}(i))^2 + \\ w_2 P_g(i)^2 + w_3 \Delta P_{fl}(i)^2 \end{cases}$$
(24)

subject to: $P_{sup}(i) = P_g(i) + P_{PV}(i) + P_W(i) + P_{fl}(i)$

Where: N_p is the prediction horizon, w_1 , w_2 , w_3 weighting factors, P_{sup} is total supplied power, $\Delta P_{FESS}(i)$ is the power rate constraint for FESS.

In summary, the algorithm flow of the AD-MPC to control an EV-FCS follows these steps:

- The asynchronous updatemechanism allows each local controller to optimize and update at different sampling rates or when communication packets are delayed, ensuring scalability for large-scale EV charging infrastructures. The decentralized structure reduces computational complexity and increases fault tolerance.
- Prediction Each local controller predicts future states using local measurements and the model of FESS-IBR dynamics
- 3) **Optimization** Solve the local MPC problem to minimize (J_i) subject to constraints.

TABLE III
RESULTS OF EV CHARGING ENERGY IN DIFFERENT SENARIOS

Scenario	P_e (kW)	P_{EV} (kW)	t_c (min)
Without FESS	11,250	321.4	18.7
With FESS	12,000	342.9	17.5
With FESS + AD-MPC	12,600	360.0	16.7

TABLE IV RECORDING OF THE FREQUENCY DEVIATION AND CHARGING TIME

Scenario	$\Delta f(Hz)$	T_{rec}	Stability
Without FESS	-0.18 Hz	Slow (>20 s)	Poor/grid
With FESS	-0.09 Hz	Moderate	Improved damping
FESS/AD/MPC	-0.06 Hz	Fast ($\sim 6 \text{ s}$)	Excellent

- 4) **Asynchronous Update** Apply the most recent control input $(u_i(k))$ even if neighboring subsystems have not updated.
- Coordination Exchange limited information (power and state of charge) between neighboring units to ensure system-wide balance.
- Reiteration Repeat the process at the next sampling instant.

VI. CASE STUDY

The proposed case study focuses on FCS integrated within a low-inertia power system. The system consists of three major components: LFC unit connected to the main grid, supplying 10 MW of power; IBR, which includes a WECS and a PV plant, jointly providing an additional 1.25 MW; and 15 FESS rated at 100 kW each, capable of delivering up to 1.5 MW total. During peak demand conditions, the FESS units supply 50 % of their rated capacity (750 kW) to support the charging station. The FCS is designed to accommodate 35 EVs charging simultaneously, each at a fast-charging rate of 350 kW and an average energy requirement of 100 kWh per session.

VII. RESULTS AND DISCUSSION

A. Impact of FESS on the EV Power Density

The first sets of results evaluate the impact of FESS and the AD-MPC controller. To do so, the system without FESS, the system with FESS, and the system with FESS and AD-MPC are evaluated. Without FESS, charging takes the longest. With FESS: FESS contributes 750 kW, boosting available power as shown in Fig. 3 and reducing charge time Fig. 4 by 7 %, With FESS + AD-MPC, the dynamic coordination is improved by 5 % gain further reducing charge time by 10 % overall. The recapitulation of results is shown in the Table. III where P_T is the total power, P_{EV} is the total power per EV, t_c charging time.

B. Impact of Many EV Charging Simultaneously on the Grid Frequency

When multiple EVs charge simultaneously, the sudden increase in load leads to a significant impact on the grid frequency, resulting in noticeable frequency deviations. To assess the effect of this load fluctuation, the grid frequency

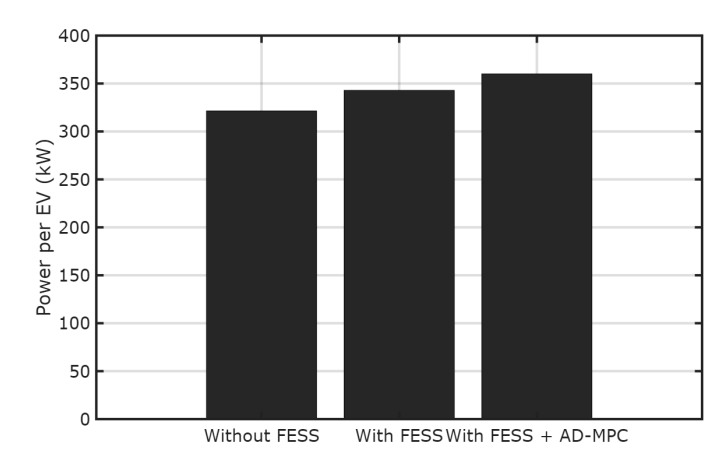


Fig. 3. Power Density for EV Charging under Different Scenarios

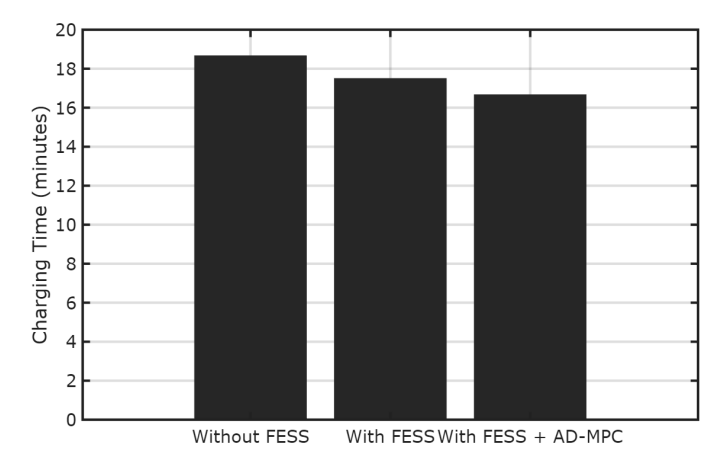


Fig. 4. EV charging Time under different scenarios

response is evaluated under three scenarios: without FESS support, with FESS integration, and with FESS controlled using AD-MPC, as shown in Fig. 5, and the results are summarized in a Table. 5.

When 35 EVs (350 kW each) start charging, the grid frequency drops due to a sudden increase in 12.25 MW load. FESS mitigates this by rapidly injecting stored energy

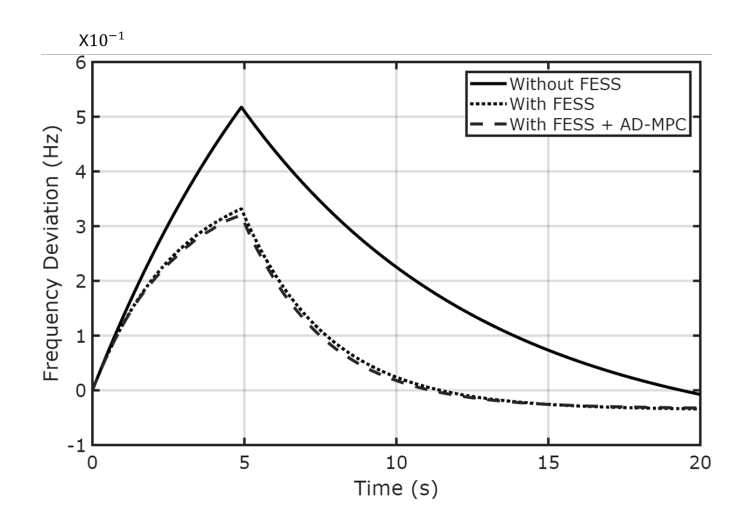


Fig. 5. Initial Frequency Dynamics during EV Charging

from FESS, improving frequency recovery. AD-MPC further optimizes FESS dispatch asynchronously across subsystems, reducing overshoot and enhancing overall system stability. This study confirms that the combination of FESS and AD-MPC can transform the operation of EV charging networks from passive loads into active, grid-supportive systems.

VIII. CONCLUSION AND RECOMMENDATIONS FOR FUTURE TRENDS

This study demonstrated that integrating FESS with AD-MPC significantly enhances the stability and efficiency of EV smart charging stations powered by IBRs. The proposed system minimized frequency deviations, improved power density, and reduced charging time, showing clear advantages over conventional configurations without FESS.

The findings indicate that FESS technology can serve as a fast response and durable energy buffer for the EV, making it ideal for mitigating grid instability caused by large-scale EV adoption in South Africa. Looking ahead, future trends should focus on real-time hardware implementation, AI-driven predictive control optimization, and hybrid energy integration strategies combining PV solar, WECS, and kinetic storage. These directions will advance the development of resilient, low-carbon, and intelligent EV charging infrastructures aligned with South Africa's 2030 energy transition goals.

The proposed control strategy not only mitigates frequency deviations during peak demand but also reduces the average charging time per vehicle by maintaining a stable power density. Hence, the proposed hybrid configuration represents a sustainable and high-performance solution for the integration of renewable energy sources and large-scale EV charging in South Africa's low-inertia power grid.

REFERENCES

- [1] International Energy Agency, "Global ev outlook 2024," 2024. [Online]. Available: https://www.iea.org/reports/global-ev-outlook-2024
- [2] A. Choudhury et al., "Flywheel energy storage systems: A critical review on technologies, applications, and future prospects," *International Transactions on Electrical Energy Systems*, vol. 31, no. 9, p. e13024, 2021.
- [3] Forbes Africa, "What's the the down road for market in south africa?" 2023. [Online]. Available: https://www.forbesafrica.com/driving-ambition/2023/09/13/ whats-down-the-road-for-the-ev-market-in-south-africa
- [4] Danish Energy Agency, "Technology data catalogue for energy storage," Energy Technology Data Catalogue, Tech. Rep., 2023.
 [Online]. Available: https://ens.dk/sites/ens.dk/files/Analyser/version_ 06_-_technology_data_catalogue_for_energy_storage_0.pdf
- [5] Q. Xu, W. Teng, R. Qin, S. Song, Y. Liu, and S. Liang, "Energy management and control strategy for grid-connected frequency regulation flywheel energy storage systems," *Energy Storage Science and Technology*, vol. 14, no. 2, pp. 567–580, 2025.
- [6] REN21, "Renewables 2024 global status report," 2024. [Online]. Available: https://www.ren21.net/reports/global-status-report
- [7] D. G. Dorrell, W. Xu, A. F. Flores Filho, and M. Brown, "High-power low-energy flywheels for power system support: A review," in *IECON* 2020 The 46th Annual Conference of the IEEE Industrial Electronics Society. IEEE, 2020, pp. 1003–1008.
- [8] E. News. (2025, July) Sa's fully electric fleet to reach 22,500 cars by 2030 - report. Accessed: 2025-10-03. [Online]. Available: https://www.engineeringnews.co.za/article/sas-fully-electric-fleet-to-reach-22500-cars-by-2030-report-2025-07-25
- [9] M. . Guardian. (2022, July) Bmw i4 m50 and ix3 officially in south africa. Accessed: 2025-10-02. [Online]. Available: https://mg.co.za/ motoring/2022-07-25-bmw-i4-m50-and-ix3-officially-in-south-africa/

- [10] F. M. Company. (2023, March) Ford celebrates 100 years in south africa, announces ranger phev investment, new products and legacy csr projects. Accessed: 2025-10-02. [Online]. Available: https://media.ford.com/content/fordmedia/img/za/en/news/2023/ 03/Ford-Celebrates-100Years-in-South-AfricaAnnouncesRanger.html
- [11] ITWeb. (2019, October) Mercedes-benz shows off luxury new electric vehicle in sa. Accessed: 2025-10-02. [Online]. Available: https://www.itweb.co.za/article/mercedes-benz-shows-off-luxury-new-electric-vehicle-in-sa/mYZRX79PjQwvOgA8
- [12] V. S. Africa. (2024, July) Volkswagen id.4 available in south africa as a test fleet. Accessed: 2025-10-03. [Online]. Available: https://www.vw.co.za/en/volkswagen-experience/newsroom/ Volkswagen-ID-4-available-in-South-Africa-as-a-test-fleet.html
- [13] News24. (2013, November) 2013 nissan leaf in sa. Accessed: 2025-10-03. [Online]. Available: https://www.news24.com/life/ 2013-nissan-leaf-in-sa-20131122
- [14] MyBroadband. (2024, October) First electric toyota gets south african launch date. Accessed: 2025-10-03. [Online]. Available: https://mybroadband.co.za/news/motoring/ 522805-first-electric-toyota-gets-south-african-launch-date.html
- [15] I. S. Africa. (2024, August) Isuzu to tease new n-series ev truck at kragdag expo. Accessed: 2025-10-03. [Online]. Available: https://www.isuzu.co.za/newsroom/isuzu-to-tease-new-n-series-ev-truck-at-kragdag-expo
- [16] C. Matos, E. Rosales-Asensio, J. A. Carta, and P. Cabrera, "Flywheels in renewable energy systems: An analysis of their role in managing intermittency," *Journal of Energy Storage*, vol. 122, p. 116674, 2025.
- [17] B. Sun, T. Dragičević, F. D. Freijedo, J. C. Vasquez, and J. M. Guerrero, "A control algorithm for electric vehicle fast charging stations equipped with flywheel energy storage systems," *IEEE Transactions on Power Electronics*, vol. 31, no. 9, pp. 6674–6685, 2015.
- [18] P. Mouratidis, "Augmenting electric vehicle fast charging stations with battery-flywheel energy storage," *Journal of Energy Storage*, vol. 97, p. 112957, 2024.
- [19] S. Wen, Y. Gong, X. Mu, S. Zhao, and C. Wang, "Optimal configuration of flywheel-battery hybrid energy storage system for smoothing windsolar power generating fluctuation," *Energies*, vol. 18, no. 8, p. 2055, 2025.
- [20] E. Camacho and C. Bordons, Model Predictive Control, 2nd ed. Springer, 2013.
- [21] W. Ngaha, D. Dorrell, and J. V. Coller, "Integration of flywheel energy storage system and model predictive control for smart charging station applications," 2025, under Review, Journal of Energy.
- [22] K. Xu, Y. Guo, G. Lei, and J. Zhu, "A review of flywheel energy storage system technologies," *Energies*, vol. 16, no. 18, p. 6462, 2023.
- [23] GreenCape. (2025, April) Electric vehicles market intelligence report 2025 — south africa. Projected SA fully electric fleet to reach 22,500 cars by 2030. Accessed: 2025-10-10. [Online]. Available: https://greencape.co.za/market-intelligence/electric-vehicles/
- [24] Y. Wang, J. Zhang, G. Tian, and G. Liu, "Model predictive control strategy of flywheel energy storage system based on matrix converter," *Journal of Electrical Engineering*, vol. 19, no. 2, pp. 26–33, 2024. [Online]. Available: https://doi.org/10.11985/2024.02.004
- [25] E. Muljadi and C. Butterfield, "Pitch-controlled variable-speed wind turbine generation," *IEEE Transactions on Industry Applications*, vol. 37, no. 1, pp. 240–246, 2001.
- [26] Department of Energy South Africa, "Integrated resource plan (irp 2019)," https://www.energy.gov.za/IRP/irp-2019.html, 2019, accessed: 2025-10-10.
- [27] Council for Scientific and Industrial Research (CSIR), "Statistics of utility-scale power generation in south africa 2021," 2021, accessed: 2025-10-10.